Proceedings of the
47th IEEE Conference on Decision and Control
Cancun, Mexico, Dec. 9-11, 2008

Physical Modeling and Control of Homogeneous Charge Compression Ignition (HCCI) Engines

Anders Widd, Per Tunestål, and Rolf Johansson

Abstract— **Due to the possibility of increased efficiency and reduced emissions, Homogeneous Charge Compression Ignition (HCCI) is a promising alternative to conventional internal combustion engines. Ignition timing in HCCI is highly sensitive to operating conditions and lacks direct actuation, making it a challenging subject for closed-loop control. This paper presents results on model-based control of ignition timing and work output using a cycle-resolved physical model including cylinder wall temperature dynamics. The model was used to design model predictive controllers for simultaneous control of the ignition timing and the indicated mean effective pressure by varying the inlet valve closing and the intake temperature. The performance of the resulting controller was evaluated in simulation and two possible extensions were developed. An extended controller was validated on a real engine.**

I. INTRODUCTION

Homogeneous Charge Compression Ignition (HCCI), or Controlled Auto-Ignition (CAI), is a promising alternative to conventional internal combustion engines due to the possibility of increased efficiency and reduced emissions. A great challenge with HCCI is control of the combustion phasing, mainly due to the lack of direct actuation. Ignition timing in HCCI engines is determined by several factors [1]; the auto-ignition properties of the air-fuel mixture, the intake temperature, the amount of residual gases in the cylinder, etc. Several possible control signals have been evaluated [1], such as variable valve timing, intake temperature, and the amount of residuals trapped in the cylinder.

Heat transfer effects between the in-cylinder charge and the cylinder walls are important for explaining HCCI cycle-to-cycle behavior [2]. However, many modeling approaches for control only consider heat transfer from the gases to the walls and assume a fixed cylinder wall temperature [1]. Continuous-time models including cylinder wall temperature were presented in [2], [3]. The former also presented results on model-based control. Two recent examples of cycle-resolved models of HCCI used for closed-loop control are [4], [5]. The models contain a cycle-to-cycle coupling through the residual gas temperature, also included in the current model. However, when there is only little residuals present in the cylinder it is more physically reasonable to let the cylinder wall temperature link the cycles.

The model used in this work, [6], is an extension of the model in [4] as it uses the same basic formulation with the addition of cylinder wall temperature dynamics and with a few modifications. The outputs were chosen to be Indicated Mean Effective Pressure (IMEP_n) and the crank angle of 50% burnt (θ_{50}). This choice was justified by the fact that IMEP_n relates to the work output of the engine and that θ_{50} was shown to be a robust indicator of combustion phasing [7]. The inputs were the intake temperature (T_{in}) and the crank angle of inlet valve closing (θ_{IVC}).

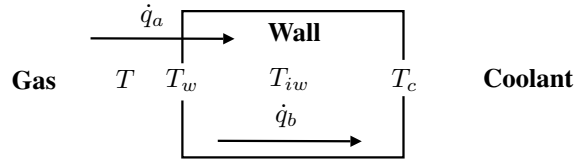

Fig. 1. Principle of the cylinder wall model.

The paper outline is as follows: The model is reviewed in Sec. II, and model calibration results are given in Sec. III. The nominal control design is outlined in Sec. IV with evaluations and extensions in Sec. V. Finally, some concluding remarks are given.

II. PHYSICAL MODEL

In this section, the physical model is outlined, for further details see [6]. The model assumed isentropic compression and expansion and heat transfer between the in-cylinder charge and the cylinder walls was modeled as three events during each cycle; after mixing, after combustion, and after expansion. This approach allows tracking of the temperature dynamics of gas and cylinder wall during the cycle while keeping the complexity low. A list of frequently used parameters and variables is shown in Table I.

A. Cylinder Wall Temperature Dynamics

The cylinder wall was modeled as a single-zone system, where it was assumed that the outer surface of the cylinder wall was maintained at a constant temperature, T_c, and that convection occured between the in-cylinder gases and the cylinder wall, see Fig 1. The first law of thermodynamics applied to the gas when no work is performed yields the expression $\dot{T} = -\dot{q}_a/mC_v$ where T, m, and C_v are the temperature, mass, and specific heat of the gas. The heat flow was modeled using the Newton law $\dot{q}_a = h_c A_c(T - T_w)$ where h_c is the convection coefficient, A_c is the wall surface area and T_w is the wall surface temperature. The inner wall temperature, T_{iw}, has a time derivative given by $\dot{T}_{iw} = (\dot{q}_a - \dot{q}_b)/m_c C_p$ where C_p is the specific heat of the cylinder wall, m_c is the cylinder wall mass, and $\dot{q}_b$ is the

A. Widd and R. Johansson are with the Department of Automatic Control, Lund University, Box 118 SE 221 00 Lund, Sweden. {Anders.Widd | Rolf.Johansson}@control.lth.se

P. Tunestål is with the Division of Combustion Engines, Department of Energy Sciences, Lund University, Box 118 SE 221 00 Lund, Sweden. Per.Tunestal@energy.lth.se

978-1-4244-3124-3/08/$25.00 ©2008 IEEE

TABLE I
LIST OF PARAMETERS AND VARIABLES

Parameter	Definition
A_a	Arrhenius scaling factor
A_c	Cylinder wall area, [m^2]
α	Molar fraction of exhaust gases
C_v	Gas heat capacity, [J/kgK]
C_p	Cast iron heat capacity [J/kgK]
E_a	Arrhenius activation energy, [J/kg]
ϕ	Equivalence ratio
γ	Specific heat ratio
h_c	Convective heat transfer coefficient, [W/m^{2}K]
IMEP$_n$	Indicated mean effective pressure, [Pa]
k_c	Conductive heat transfer coefficient, [W/mK]
L_c	Cylinder wall thickness, [m]
m	Gas mass, [kg]
m_a	Air mass, [kg]
m_c	Cylinder wall mass [kg]
m_f	Fuel mass, [kg]
n	Arrhenius sensitivity to pressure
P_{in}	Intake pressure, [Pa]
Q_{LHV}	Lower heating value of isooctane, [J/kg]
R	Gas constant, [J/kg/K]
T	Gas temperature, [K]
T_c	Coolant temperature, [K]
T_{in}	Intake temperature, [K]
T_{iw}	Cylinder wall inner temperature, [K]
T_w	Cylinder wall surface temperature, [K]
θ_{50}	Crank angle of 50% burnt, [rad]
θ_{IVC}	Crank angle of inlet valve closing, [rad]
θ_{TDC}	Crank angle at top dead center, [rad]
V_d	Displacement volume, [m^3]

conductive heat flow through the wall. This flow is given by $\dot{q}_b = (T_w - T_c)k_c A_c/L_c$ where k_c is the conduction coefficient and L_c is the wall thickness. Assuming that the steady-state temperature condition $T_{iw} = (T_w + T_c)/2$ holds the temperature equations may be written as

$$\dot{\mathcal{T}} = A_{ht}\mathcal{T} + B_{ht}T_c, \tag{1}$$

where

$$A_{ht} = \begin{bmatrix} -\frac{h_c A_c}{mC_v} & \frac{h_c A_c}{mC_v} \\ 2\frac{h_c A_c}{m_c C_p} & -2\frac{h_c A_c + k_c A_c/L_c}{m_c C_p} \end{bmatrix}, \quad B_{ht} = \begin{bmatrix} 0 \\ 2\frac{k_c A_c}{L_c m_c C_p} \end{bmatrix}, \quad \mathcal{T} = \begin{bmatrix} T \\ T_w \end{bmatrix} \tag{2}$$

If T_c is assumed to be slowly varying, the temperature at time t_i can be computed using a zero-order-hold approach

$$\mathcal{T}(t_i) = \Phi_i \mathcal{T}(0) + \Gamma_i T_c, \tag{3}$$

where [8]

$$\Phi_i = e^{A_{ht}t_i}, \quad \Gamma_i = \int_0^{t_i} e^{A_{ht}(t_i-\tau)} B_{ht} d\tau \tag{4}$$

Eq. (3) was used to update the gas temperature and the wall temperature after mixing, after combustion, and after expansion. Since the integration time t_i needs to be adapted to each instant and also some of the parameters depend on operating conditions, three sets of matrices $\{\Phi_i, \Gamma_i\}$, $i = 1, 3, 5$ were used, where $i = 1$ corresponded to mixing, $i = 3$ corresponded to combustion, and $i = 5$ corresponded to expansion.

B. Temperature Trace

In this section the evolution of the gas temperature, the pressure, and the wall temperature during an engine stroke is presented. Indices in parentheses denote cycle number while subscripts denote stages within the cycle. For example, $T_1(k)$ denotes the gas temperature after mixing in cycle k. The subscript '+' is added to the temperatures after Equation (3) has been applied to model heat transfer, e.g. $T_{1+}(k)$.

1) Intake/Mixing: The gas temperature at the start of cycle k, $T_1(k)$, was modeled as the weighted average of the intake temperature and the temperature of the residuals, cf. [4];

$$T_1(k) = \frac{C_{v,in}T_{in}(k) + C_{v,EGR}\chi\alpha T_{5+}(k-1)}{C_{v,in} + \alpha C_{v,EGR}}, \tag{5}$$

where $C_{v,in}$ and $C_{v,EGR}$ are the specific heats of the fresh reactants and the residual gases respectively and α is the molar ratio between residuals and inducted gases. The final gas temperature of cycle $k-1$ is denoted $T_{5+}(k-1)$, and χ is a measure of how much the residual temperature has decreased. The initial wall temperature of cycle k was set equal to the final wall temperature of cycle $k-1$;

$$T_{w1}(k) = T_{w5+}(k-1) \tag{6}$$

Eq. (3) with $i = 1$ was applied to yield new temperatures $T_{1+}(k)$ and $T_{w1+}(k)$;

$$\begin{bmatrix} T_{1+}(k) \\ T_{w1+}(k) \end{bmatrix} = \Phi_1 \begin{bmatrix} T_1(k) \\ T_{w1}(k) \end{bmatrix} + \Gamma_1 T_c \tag{7}$$

2) Compression: Isentropic compression was assumed so that the gas temperature and pressure after compression, $T_2(k)$ and $P_2(k)$, were given by

$$T_2(k) = T_{1+}(k)\left(\frac{V_1(k)}{V_2(k)}\right)^{\gamma-1}, \quad P_2(k) = P_{in}\left(\frac{V_1(k)}{V_2(k)}\right)^{\gamma} \tag{8}$$

where P_{in} is the intake pressure, γ is the specific heat ratio, $V_1(k)$ is the cylinder volume at inlet valve closing, and $V_2(k)$ is the cylinder volume when combustion is initiated. The volumes were calculated from the crank angle using geometric data on the engine [9].

3) Combustion: The crank angle of auto-ignition, $\theta_{ign}(k)$, was modeled using an Arrhenius-type integral independent of species concentration [10], so that the condition

$$\int_{\theta_{IVC}(k)}^{\theta_{ign}(k)} f_k(\theta) d\theta = 1 \tag{9}$$

was fulfilled with

$$f_k(\theta) = A_a P_{in}^n \mathcal{V}_k(\theta)^{\gamma n} \exp\left(-\frac{E_a \mathcal{V}_k(\theta)^{1-\gamma}}{RT_{1+}(k)}\right). \tag{10}$$

The parameter A_a is a scaling factor, E_a is the activation energy for the reaction, n is the reaction sensitivity to pressure, R is the gas constant, and $\mathcal{V}_k(\theta) = V_1(k)/V(\theta)$. To simplify this expression an approach similar to that in [4] was taken. The integrand was approximated with its maximum value, which is attained at Top Dead Center (TDC). The corresponding crank angle degree (CAD) was denoted θ_{TDC},

so that $f_k(\theta) = f_k(\theta_{TDC})$. The lower integration limit was then shifted from θ_{IVC} to θ_{TDC} and the resulting integral equation was solved for $\theta_{ign}(k)$;

$$\theta_{ign}(k) = \Delta\theta_A + \frac{1}{f_k(\theta_{TDC})} \tag{11}$$

where $\Delta\theta_A$ is an offset in CAD.

The temperature after combustion was calculated as

$$T_3(k) = T_2(k) + \frac{Q_{LHV}}{(1+\alpha)(\phi^{-1}(m_a/m_f)_s + 1)C_v} \tag{12}$$

where Q_{LHV} is the lower heating value of isooctane, ϕ is the equivalence ratio, and $(m_a/m_f)_s$ is the stoichiometric air-to-fuel ratio. The denominator approximates the ratio between the total in-cylinder mass and the fuel mass [6]. Eq. (3) was then applied with $i = 3$ and $T_{w3}(k) = T_{w1+}(k)$ to find new temperatures $T_{3+}(k)$, $T_{w3+}(k)$. The pressure after combustion is

$$P_3(k) = \frac{T_{3+}(k)}{T_2(k)} P_2(k) \tag{13}$$

4) Expansion: The gas temperature and pressure after expansion was calculated assuming adiabatic expansion.

$$T_4(k) = T_{3+}(k)\left(\frac{V_2(k)}{V_4(k)}\right)^{\gamma-1}, \quad P_4(k) = P_3(k)\left(\frac{V_2(k)}{V_4(k)}\right)^{\gamma} \tag{14}$$

As the exhaust valve opens, the pressure drops to the surrounding pressure and there is a further decrease in temperature,

$$T_5(k) = T_4(k)\left(\frac{P_{in}}{P_4(k)}\right)^{(\gamma-1)/\gamma} \tag{15}$$

Finally, Eq. (3) was applied with $i = 5$ and $T_{w5}(k) = T_{w3+}(k)$ to obtain the final gas temperature $T_{5+}(k)$ and the final wall temperature $T_{w5+}(k)$.

C. Model States and Output Equations

The states are the final gas temperature, $T_{5+}(k)$, and the final wall temperature, $T_{w5+}(k)$. Other choices are possible but at least two variables are needed to fully describe the state. Further, it is possible to use other control variables, such as the amount of residuals or the equivalence ratio without altering the model. Assuming that combustion proceeds as a function of crank angle the following holds, where $\Delta\theta$ is an offset in CAD;

$$\theta_{50}(k) = \theta_{ign}(k) + \Delta\theta \tag{16}$$

IMEP_n was calculated from the gas temperatures [9];

$$\text{IMEP}_n(k) = \frac{mC_v}{V_d}\left(T_{1+}(k) - T_2(k) + T_{3+}(k) - T_4(k)\right) \tag{17}$$

where V_d is the displacement volume.

III. Model Calibration

The model was calibrated using measurement data from a single-cylinder engine equipped with a piston glass allowing measurements of the wall temperature to be made using thermographic phosphor [11]. The calibration was done using optimization techniques, as outlined in [6]. Only parameters connected to the heat transfer equations and the auto-ignition were optimized. A stationary operating point was used for the calibration and the model was validated dynamically during a step in the equivalence ratio. Fig. 2 shows the model outputs and the wall temperature during a positive step in the equivalence ratio ϕ. The model captured the qualitative and quantitative behaviour of all three variables.

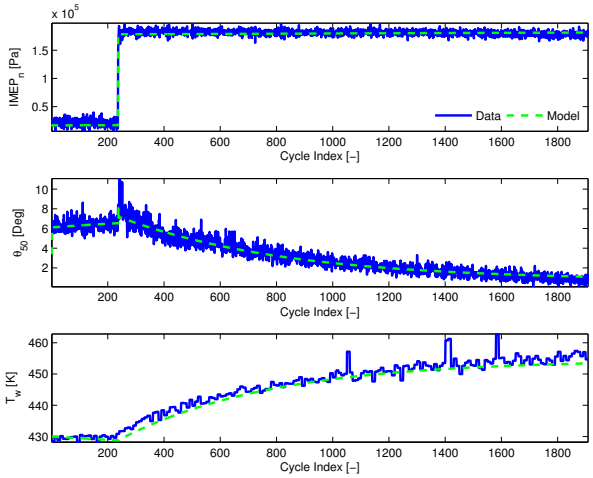

Fig. 2. IMEP_n, θ_{50}, and T_w measured and model output during a step in equivalence ratio. Figure reproduced from [6].

IV. Control Design

This section briefly reviews the fundamentals of Model Predictive Control (MPC) and outlines the control design.

A. Model Predictive Control

Model predictive control [12] was shown to be a suitable control strategy for HCCI [13] due to its MIMO-capabilities and its ability to handle explicit constraints on control signals and outputs. The following review is based on [12].

Consider the cost function

$$J(k) = \sum_{i=H_w}^{H_p+H_w-1} \mathcal{Y}(i|k) + \sum_{i=0}^{H_u-1} \mathcal{U}(i|k) \tag{18}$$

where

$$\begin{aligned} \mathcal{Y}(i|k) &= ||\hat{y}(k+i|k) - r(k+i|k)||_Q^2, \\ \mathcal{U}(i|k) &= ||\Delta\hat{u}(k+i|k)||_R^2 \end{aligned} \tag{19}$$

and $\hat{y}(k+i|k)$ is the predicted output at time $k+i$ given a measurement at time k, $\Delta\hat{u}(k+1|k)$ is the predicted change in control signal, and $r(k+i|k)$ is the set point at time $k+i$. The parameters H_w, H_p, and H_u define the length and offset of the prediction horizon and the length of the control horizon. At each sample, the cost function in (18)

is minimized by determining a sequence of changes to the control signal $\Delta u(k+i|k)$, $i = 0 \dots H_u$, subject to the constraints

$$y_{min} \leq \quad y(k) \quad \leq y_{max} \tag{20}$$
$$u_{min} \leq \quad u(k) \quad \leq u_{max} \tag{21}$$
$$\Delta u_{min} \leq \Delta u(k) \leq \Delta u_{max} \tag{22}$$

for all k. The first step of the optimal sequence is then applied to the plant and the optimization is repeated in the next step yielding a new optimal sequence [12].

B. Control Design

To design controllers based on the model, one could linearize the equations around a set-point or a trajectory. However, as the states are not directly measurable, state estimation via the output equations would be needed. In the following section a change of coordinates is presented that allows IMEP$_n$ and θ_{50} to be used as states.

1) Change of Coordinates: Due to the simplified auto-ignition model it is possible to uniquely determine the states from the current output measurement. Solving (11) for $T_{1+}(k)$ using (10) and (16) yields

$$T_{1+}(k) = \frac{E_a \mathcal{V}_k(\theta_{TDC})^{1-\gamma}}{R \ln\left(A_a P_{in}^n \mathcal{V}_k(\theta_{TDC})^{\gamma n} \theta_m(k)\right)} \tag{23}$$

where $\theta_m(k) = \theta_{50}(k) - \Delta\theta_A - \Delta\theta$. The corresponding wall temperature can then be calculated using (3), (8), (12), (14), and (17);

$$T_{w1+}(k) = \frac{\text{IMEP}_n(k) - (mC_v/V_d)\left(c_1 T_{1+}(k) + c_2 c_3\right)}{c_3 (mC_v/V_d)\Phi_{3[1,2]}}, \tag{24}$$

where

$$c_1 = 1 - \left(\frac{V_1}{V_2}\right)^{\gamma-1} + c_3 \Phi_{3[1,1]} \left(\frac{V_1}{V_2}\right)^{\gamma-1} \tag{25}$$

$$c_2 = \frac{\Phi_{3[1,1]} Q_{LHV}}{(1+\alpha)\left(\phi^{-1}\left(\frac{m_a}{m_f}\right)_s + 1\right) C_v} + \Gamma_{3[1,1]} T_c \tag{26}$$

$$c_3 = 1 - \left(\frac{V_2(k)}{V_4(k)}\right)^{\gamma-1} \tag{27}$$

By going through the cycle the final temperatures are obtained and can be propagated to cycle $k+1$.

2) Linear Model: Due to the complexity introduced by the cross-coupling in the heat transfer instants, the resulting equations are not easily tractable by hand. However, using software capable of performing symbolic calculation a linear model on the following form was obtained;

$$y(k+1) = Ay(k) + Bu(k) \tag{28}$$

where

$$y(k) = \begin{bmatrix} \text{IMEP}_n(k) \\ \theta_{50}(k) \end{bmatrix}, \quad u(k) = \begin{bmatrix} \theta_{IVC}(k) \\ T_{in}(k) \end{bmatrix} \tag{29}$$

and

$$A = \frac{\partial y(k+1)}{\partial y(k)}(y^0, u^0), \quad B = \frac{\partial y(k+1)}{\partial u(k)}(y^0, u^0) \tag{30}$$

where (y^0, u^0) is a stationary operating point [8].

Fig. 3 shows the simulated response from the nonlinear model and that of the linearized model. The fit between the two is rapidly deteriorating with increasing distance to the linearization point. Inspired by this observation a suitable approach may be to use a piece-wise linear (sometimes referred to as linear parameter-varying) approximation of the nonlinear model containing multiple linearizations, replacing (28) with

$$y(k+1) = A_j y(k) + B_j u(k), \quad j = g(y(k)) \tag{31}$$

where $g(y(k))$ maps the current output measurement to the corresponding linearization. Using three linearizations, and switching based on the θ_{50} measurement, the L_2-error in IMEP$_n$ and θ_{50} was decreased by 26 % and 10 % respectively during the trajectory shown in Fig. 3. Control simulations based on this model will be evaluated in Sec. V.

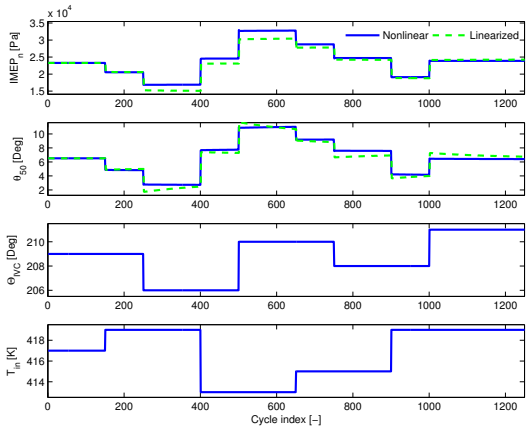

Fig. 3. IMEP$_n$ and θ_{50} from the nonlinear model and the linearization in response to the control signals θ_{IVC} and T_{in}.

3) Tuning: The linear model (28) was used to generate predictions in the MPC strategy. To ensure error-free tracking explicit integrator states were added to the linear model [14]. Constraints were added to the outputs mainly to limit deviations in combustion phasing, while the constraints on the control signals were introduced based mainly on the limitations of the actuators but also to avoid exciting unmodeled effects related to e.g. the gas exchange process. Suitable values for the prediction and control horizons were determined from simulation.

V. Controller Evaluation

This section presents the evaluation of the nominal controller and discusses two possible extensions.

A. Nominal Controller Performance

The simulated response using the nominal controller during a series of step changes in the reference values is shown in Fig. 4. The controller followed the reference trajectory for both outputs. There were some transients in θ_{50} during the step changes in IMEP$_n$. These could be partly diminished by further tuning of the controller. However, as shown in the

next section, using a controller based on the the piece-wise linear approximation suggested in Sec. IV-B.2 reduces the transients substantially.

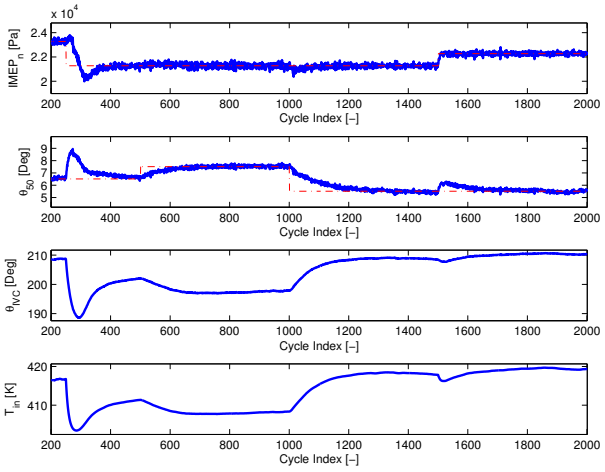

Fig. 4. Simulated IMEP$_n$, θ_{50}, and control signals θ_{IVC} and T_{in} for the nominal model predictive controller.

Another issue which needs to be addressed is the heating of intake air, which can not be done arbitrarily fast. The heater was modeled as a first order system, so that

$$T_{in}(k+1) = e^{-1/T_f} T_{in}(k) + \left(1 - e^{-1/T_f}\right) T_{in}^r(k) \quad (32)$$

where T_f is the time constant and T_{in}^r is the reference value for T_{in}. Fig. 5 shows the measured response to a step in desired intake temperature and the response of the first-order approximation in (32). It should be noted that the time constant of the heater dynamics depends on the tuning of the control loop governing the intake temperature. The simulated performance of the nominal controller was

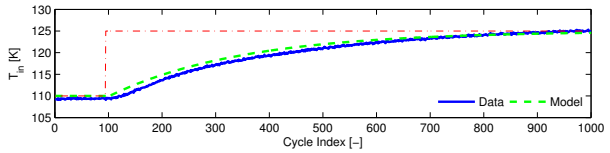

Fig. 5. Measured and simulated response to a step change in the desired intake temperature. Measurement data by courtesy of M. Karlsson.

drastically decreased when the heater-model was introduced. This is partly due to that future control moves will be based on an incorrect value of T_{in} when the heater dynamics are not accounted for. In Sec. V-C a solution to this issue, that makes use of direct measurements of $T_{in}(k)$ to calculate the coming control moves, is proposed.

B. Piece-wise Linear Approximation

As noted in Sec. IV-B.2, the fit of the linear approximation is deteriorating with increasing distance from the linearization point. Fig. 6 shows the simulated response to the nominal model predictive controller and to a switched controller based on a piece-wise linear approximation using three regions. The weights and prediction parameters were the same for both controllers. The switched controller utilized a more accurate dynamic model and yielded better performance. The transients in θ_{50} during the steps in IMEP$_n$ were reduced and the overall response was faster.

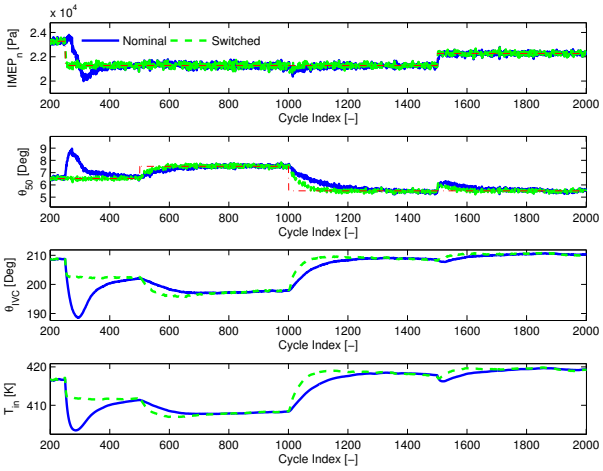

Fig. 6. Simulated IMEP$_n$, θ_{50}, and control signals θ_{IVC} and T_{in} for the nominal model predictive controller and the switched controller.

C. Extension to include Actuator Dynamics

One way of addressing the problem with dynamics in the intake temperature actuator is to include the heater model in the control design. Combining (32) and (28) yields a third-order system.

$$\begin{bmatrix} y(k+1) \\ T_{in}(k+1) \end{bmatrix} = A_e \begin{bmatrix} y(k) \\ T_{in}(k) \end{bmatrix} + B_e \begin{bmatrix} \theta_{IVC}(k) \\ T_{in}^r(k) \end{bmatrix} \quad (33)$$

where

$$A_e = \begin{bmatrix} A & B_{[:,2]} \\ 0 & e^{-1/T_f} \end{bmatrix}, \quad B_e = \begin{bmatrix} B_{[:,1]} & 0 \\ 0 & 1 - e^{-1/T_f} \end{bmatrix} \quad (34)$$

A controller was designed based on the extended model and compared to one based on the nominal model. As measurement of T_{in} is possible, the control moves were based on the actual intake temperature. In order to obtain reasonable tracking of combustion phasing using the nominal model, the penalty on IMEP$_n$ was reduced and that on the intake temperature control signal was increased. The controller based on the extended model controlled both outputs relatively fast in simulation, as shown in Fig. 7.

D. Experimental Validation

The extended controller, based on Eq. (33), was used to control a real engine, described in [2]. Fig. 8 shows experimental results during step changes in the set-point for θ_{50}. A different engine was used for the experiments, but aside from re-calibration of the model only little time was spent tuning the controller. The controller followed the set-point changes with a slight overshoot.

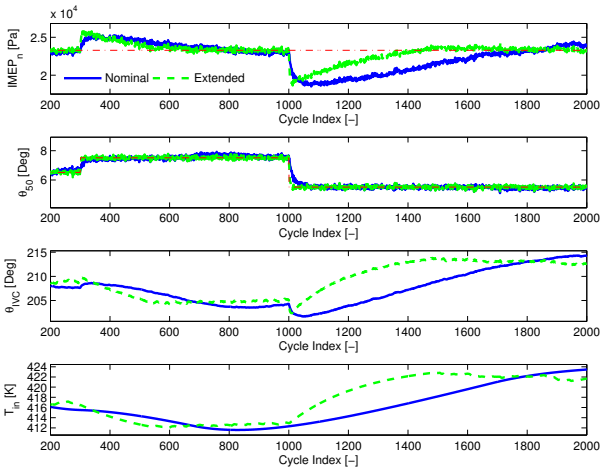

Fig. 7. Simulated IMEP$_n$, θ_{50}, and control signals θ_{IVC} and T_{in} for the nominal model predictive controller and the controller based on the extended model.

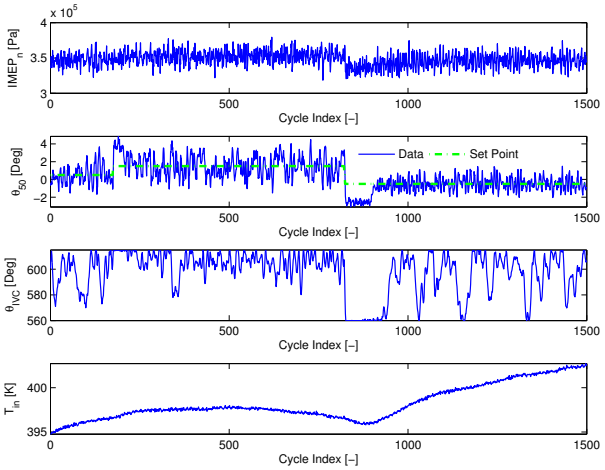

Fig. 8. Experimental IMEP$_n$, θ_{50}, and control signals θ_{IVC} and T_{in} for the extended controller on the real engine.

VI. Discussion

The piece-wise linear approximation of the model yielded good results in simulation which suggests that the approach should be pursued further and given theoretical treatment as it simplifies the control design compared to using non-linear methods directly. Introducing a simple model of the intake heater dynamics enabled simulation of a more realistic engine model for the control design. It also introduced measurements of the actual intake temperature in the extended controller. The experimental results show qualitative agreement with the simulations. A slight overshoot in θ_{50} was noted and Fig. 8 shows that the variance was larger with later combustion phasing. Future investigation of these effects involves more experimental work and implementation of the piece-wise linear controller.

VII. Conclusion

A cycle-resolved, physical model of HCCI was used to design model predictive controllers augmented with integrating states. The inclusion of cylinder wall temperature dynamics in the model provided a physically well-founded link between engine cycles when only small amounts of residuals were captured in the cylinder. A change of coordinates was introduced, enabling the measured outputs to be used as states. A linearized version of the two-input, two-output HCCI model was used to generate predictions in the MPC strategy. The performance of the resulting controller was evaluated in simulation and possible extensions were discussed. An extended version of the controller was experimentally validated on a real engine.

VIII. Acknowledgements

We are grateful for technical discussion and cooperation with D. Blom, M. Karlsson, and K. Ekholm. This research was made in the framework of KCFP, Closed-Loop Combustion Control (Swedish Energy Adm: Project no. 22485-1).

References

[1] J. Bengtsson, P. Strandh, R. Johansson, P. Tunestål, and B. Johansson, "Hybrid modelling of homogeneous charge compression ignition (HCCI) engine dynamic—A survey," *International Journal of Control*, vol. 80, no. 11, pp. 1814–1848, Nov. 2007.

[2] D. Blom, M. Karlsson, K. Ekholm, P. Tunestål, and R. Johansson, "HCCI engine modeling and control using conservation principles," *SAE Technical Papers*, no. 2008-01-0789, 2008.

[3] M. J. Roelle, N. Ravi, A. F. Jungkunz, and J. C. Gerdes, "A dynamic model of recompression HCCI combustion including cylinder wall temperature," in *Proc. IMECE2006*, Chicago, Illinois, USA, Nov. 2006.

[4] G. M. Shaver, M. Roelle, and J. C. Gerdes, "A two-input two-output control model of HCCI engines," in *Proc. 2006 American Control Conference*, Minneapolis, Minnesota, USA, June 2006.

[5] C.-J. Chiang, A. G. Stefanopoulou, and M. Jankovic, "Nonlinear observer-based control of load transitions in homogeneous charge compression ignition engines," *Control Systems Technology, IEEE Transactions on*, vol. 15, no. 3, pp. 438–448, May 2007.

[6] A. Widd, P. Tunestål, C. Wilhelmsson, and R. Johansson, "Control-oriented modeling of homogeneous charge compression ignition incorporating cylinder wall temperature dynamics," in *Proc. 9th Int. Symp. on Advanced Vehicle Control*, Kobe, Japan, Oct. 2008.

[7] J. Bengtsson, "Closed-loop control of HCCI engine dynamics," Ph.D. dissertation, Department of Automatic Control, Lund Institute of Technology, Lund University, Sweden, Nov. 2004.

[8] W. J. Rugh, *Linear System Theory - 2nd. ed.* Upper Saddle River, New Jersey: Prentice-Hall, 1996.

[9] J. B. Heywood, *Internal Combustion Engine Fundamentals*. New York: McGraw-Hill International Editions, 1988.

[10] C. Chiang and A. Stefanopoulou, "Sensitivity analysis of combustion timing and duration of homogeneous charge compression ignition (HCCI) engines," in *Proc. 2006 American Control Conference*, Minneapolis, Minnesota, USA, June 2006.

[11] C. Wilhelmsson, A. Vressner, P. Tunestål, B. Johansson, G. Särner, and M. Aldén, "Combustion chamber wall temperature measurement and modeling during transient HCCI operation," *SAE Technical Papers*, no. 2005-01-3731, 2005.

[12] J. Maciejowski, *Predictive Control with Constraints*. Essex, England: Prentice-Hall, 2002.

[13] J. Bengtsson, P. Strandh, R. Johansson, P. Tunestål, and B. Johansson, "Model predictive control of homogeneous charge compression ignition (HCCI) engine dynamics," in *2006 IEEE International Conference on Control Applications*, Munich, Germany, Oct. 2006, pp. 1675-1680.

[14] J. Åkesson, "MPCtools 1.0—Reference Manual," Dept. of Autom. Control, Lund University, Sweden, Tech. Rep. TFRT--7613, Jan. 2006.